Bioactive Materials 6 (2021) 273–284

Contents lists available at ScienceDirect

Bioactive Materials

journal homepage: http://www.keaipublishing.com/biomat

Sericin microparticles enveloped with metal-organic networks as a pulmonary targeting delivery system for intra-tracheally treating metastatic lung cancer

Jia Liu[a,1], Yan Deng[a,1], Daan Fu[a], Ye Yuan[a], Qilin Li[a,b], Lin Shi[a], Guobin Wang[c,***], Zheng Wang[a,c,**], Lin Wang[a,b,*]

[a] Research Center for Tissue Engineering and Regenerative Medicine, Union Hospital, Tongji Medical College, Huazhong University of Science and Technology, Wuhan, 430022, China
[b] Department of Clinical Laboratory, Union Hospital, Tongji Medical College, Huazhong University of Science and Technology, Wuhan, 430022, China
[c] Department of Gastrointestinal Surgery, Union Hospital, Tongji Medical College, Huazhong University of Science and Technology, Wuhan, 430022, China

ARTICLE INFO

Keywords:
Sericin microparticles
Pulmonary delivery system
Metal organic networks
Doxorubicin
Metastatic lung cancer

ABSTRACT

Chemotherapy is one of the major approaches for the treatment of metastatic lung cancer. However, systemic chemotherapy is limited by poor therapeutic efficiency and severe toxic side effects, due to the extremely low delivery efficacy and non-specificity of anticancer drugs. Herein, we report a sericin microparticles enveloped with metal-organic networks as a pulmonary delivery system for treating lung metastasis of breast cancer in an animal model. The sericin microparticles (SMPs) were prepared using water in oil (w/o) emulsification method. After doxorubicin (DOX) loading, tannic acid (TA)/ferric irons (Fe^{3+}) based metal organic networks (MON) were coated on the particles to obtain DOX-loaded microparticles (DOX@SMPs-MON). The SMPs-MON with good biocompatibility could effectively encapsulate DOX and sustainably unload cargos in a pH-dependent manner. The DOX-loaded microparticles could be uptaken by 4T1 cells, and effectively kill the cancer cells. In vivo, DOX@SMPs-MON was deposited in the lungs and remained for over 5 days after pulmonary administration. In contrast to conventional DOX treatment that did not show significantly inhibitory effects on lung metastatic tumor, DOX@SMPs-MON markedly decreased the number and size of metastatic nodules in lungs, and the lung weight and appearance were similar to those of healthy mice. In summary, the sericin microparticles with MON wrapping might be a promising pulmonary delivery system for treating lung metastatic cancer.

1. Introduction

Lung cancer, a highly invasive and fatal disease, is one of the leading causes of cancer-related deaths worldwide [1], and notably, over 70% of lung-cancer deaths are caused by metastatic lung cancers [2,3]. For treating metastatic lung cancers, chemotherapy is a major approach to control symptoms and to prolong patient survival [4,5]. Intravenous administration of chemotherapeutic agents is the mainstay of chemotherapy. However, systemic administration of anticancer drugs lacks targeting capability, causing an ineffective drug accumulation at tumorous sites and undesirable distributions in normal organs, thus leading to poor therapy efficacy and severe systemic toxicity [6].

Pulmonary administration is a promising approach to directly deliver drugs to lungs locally [7–10]. Compared with systemic therapy, pulmonary delivery offers great advantages for treating lung cancers, including (1) facilitating drug accumulation at lungs [10–13], (2) limiting the systemic distribution of anticancer drugs to avoid associated toxic side-effects, and (3) decreasing patients' pain due to non-invasive

Peer review under responsibility of KeAi Communications Co., Ltd.
* Corresponding author. Research Center for Tissue Engineering and Regenerative Medicine, Union Hospital, Tongji Medical College, Huazhong University of Science and Technology, Wuhan, 430022, China.
** Corresponding author. Research Center for Tissue Engineering and Regenerative Medicine, Union Hospital, Tongji Medical College, Huazhong University of Science and Technology, Wuhan, 430022, China.
*** Corresponding author. Department of Gastrointestinal Surgery, Union Hospital, Tongji Medical College, Huazhong University of Science and Technology, Wuhan, 430022, China.
E-mail addresses: wgb@hust.edu.cn (G. Wang), zhengwang@hust.edu.cn (Z. Wang), lin_wang@hust.edu.cn (L. Wang).
[1] These authors contributed equally to this work.

https://doi.org/10.1016/j.bioactmat.2020.08.006
Received 18 June 2020; Received in revised form 5 August 2020; Accepted 6 August 2020

needle-free treatment [14,15]. Moreover, the local delivery route increases drug retention in lungs with prolonged half-life and improved drug concentration; thus a lower dose of drug is therapeutically sufficient, which would help reduce side effects [14].

Conventional chemotherapeutic agents via pulmonary administration are rapidly cleared from lungs, which need to dose frequently to reach high concentration in terms of treating lung cancer cells, thus often inevitably increasing the risk of pulmonary toxicity [16]. To circumvent this drawback of conventional drugs, microparticles (MPs) based pulmonary drug delivery systems have emerged [17]. Such a delivery approach is thought to enhance drug accumulation and retention in lungs, sustain drug release, and decrease dosing frequency, thus improving therapy outcomes [18]. A variety of microparticles have been fabricated as pulmonary delivery systems for treating lung cancers using synthetic or natural polymers, such as polylactic-co-glycolic acid (PLGA) [19–21], polylactic acid (PLA) [22], alginate [23], and hyaluronic acid (HA) [24]. However, some properties of these microparticles are not ideal for pulmonary drug delivery: the degradation products of PLGA and PLA are reported to cause serious inflammatory responses [25,26]; and burst drug release often occurs at the initial release stage from these microparticles [27]. Thus, it is highly desired to generate a microparticles-based pulmonary drug delivery system capable of on-demand release of drugs for treating lung cancers.

Sericin is a natural protein extracted from silkworm cocoons. Due to its good biocompatibility, biodegradability, low-immunogenicity and natural cell adhesion [28,29], sericin has been widely used to develop tissue engineering scaffolds or nanocarriers for drug delivery [30–35], as well as the silk fibroin [36,37]. Hence, we proposed to prepare a pulmonary delivery system composed of (1) sericin microparticles (SMPs) as the core carrier, that can effectively encapsulate anticancer drug, and (2) tannic acid (TA) and ferric irons (Fe^{3+}) based metal-organic networks (MON) coating on SMPs (Scheme 1). Three main designing features for this metal-organic networks enveloped sericin microparticles system includes: (1) the system is fabricated by biocompatible materials, including sericin (a biocompatible and degradable protein) [38], TA (a natural polyphenol from green tea) [39] and ferric irons (an ion exist in human body) [40]; (2) MON is simply coated on SMPs in a layer-by-layer manner, which could easily control the drug release rate by adjusting the coating cycles; (3) TA-Fe^{3+} MON is stable on neutral and alkaline conditions and gradually degrades in acidic environment [41], which could prevent the drug premature leakage in normal tissues while effectively unload cargos in response to the acidic tumor and intracellular-microenvironments.

According to the above design rationales, we prepared a sericin-based microparticles (~4.6 μm) by water in oil (w/o) single emulsion method, and further coated the particles with TA-Fe^{3+} MON (SMPs-MON) (Scheme 1). The SMPs-MON exhibited great biocompatibility, effectively encapsulated doxorubicin (DOX, an anticancer drug), and sustainably released DOX in a pH-dependent manner. The DOX-loaded SMPs-MON (DOX@SMPs-MON) spread throughout the lungs and stayed more than 5 days after intratracheal administration. In the 4T1 metastatic tumor bearing mice, DOX@SMPs-MON markedly reduced the number of metastasis foci and decreased the size of nodules, and did not induce systemic toxicity. Thus, the SMPs-MON might serve as a promising pulmonary delivery system for treating lung metastatic cancer.

2. Materials and methods

2.1. Materials

Silkworm cocoons (*Haoyue*) were kindly provided by the Sericultural Research Institute, China Academy of Agriculture Science (Zhenjiang, Jiangsu, China). Sodium carbonate (Na_2CO_3) were purchased from Sinopharm Chemical Reagent Co, Ltd. (China). Doxorubicin hydrochloride (DOX) was provided by Meilun Biology Technology Co. Ltd (Dalian, China). Cellulose dialysis membranes (MWCO: 3500 Da) were purchased from Spectrum Laboratory, Inc. (Rancho DomingueZ, CA). Tannic acid (TA) and ferric chloride ($FeCl_3{\cdot}6H_2O$) were obtained from Energy Chemical (China).

2.2. Extraction of silk sericin

Silk sericin was isolated from silkworm cocoons (*Haoyue*) by

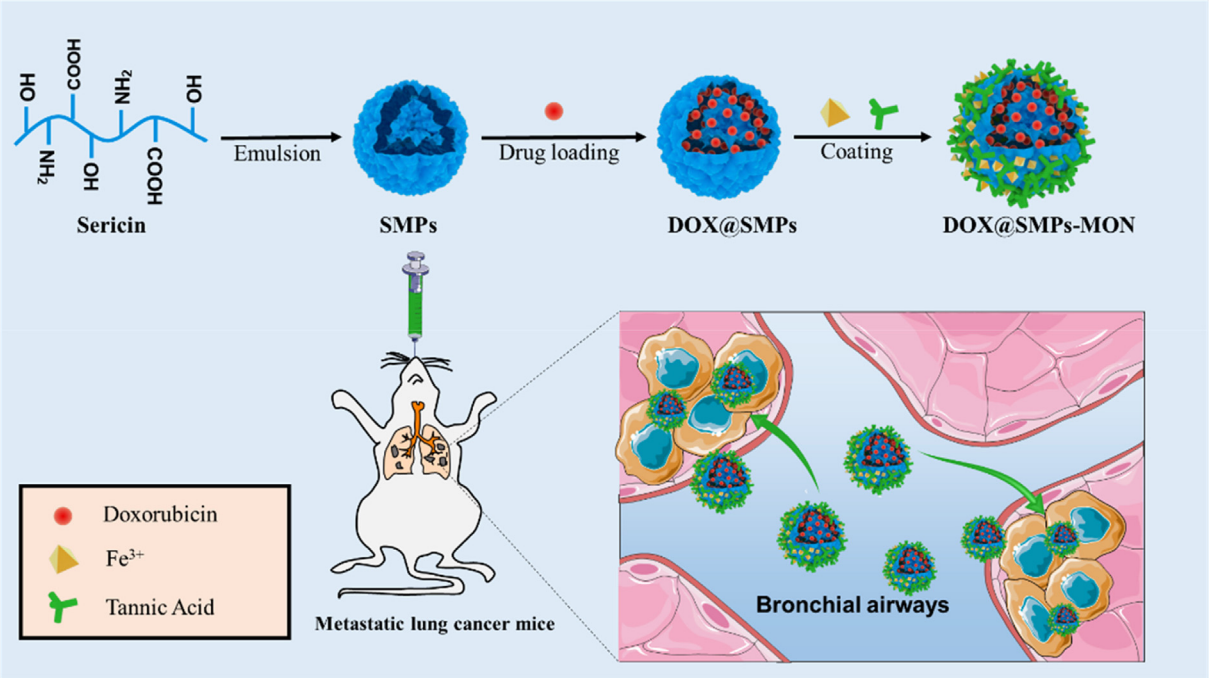

Scheme 1. Preparation and DOX loading of sericin-based microparticles with TA-Fe^{3+} metal-organic networks (DOX@SMPs-MON), and the intratracheal delivery to lung metastatic cancer.

alkaline degumming method as previously described [42]. Briefly, cocoons (0.5 g) were cut into pieces and boiled in Na_2CO_3 solution (0.02 M, 30 mL) for 1 h. Silk fibroin was removed by centrifuging at 3500 rpm for 8 min, and the supernatants were collected and dialyzed (MWCO: 3500 Da) against distill water for 48 h. Then the solutions were lyophilized to obtain silk sericin.

2.3. Synthesis of sericin microparticles (SMPs)

Sericin microparticles (SMPs) were prepared using water-in-oil (w/o) single emulsion method. Typically, sericin aqueous solution (10% wt, 1 mL) was added dropwise into corn oil (10 mL) containing Tween 20 (0.2 mL). Then, it was homogenized (800 rpm, 15 min) to obtain an emulsion. Subsequently, glutaraldehyde (25%, 0.1 mL) was added to the emulsion as a crosslinking agent and the mixture was stirred continuously for 2 h. The resulting emulsion was suspended in acetone (300 mL) and stirred gently for 40 min to allow complete solidify. Finally, the microparticles were collected by centrifugation, washed with acetone, and dried under vacuum.

2.4. Doxorubicin (DOX) loading and metal-organic networks (MON) coating

To encapsulate DOX in SMPs, doxorubicin hydrochloride (DOX, 10 mg) were dissolved in PBS (pH 8.5, 10 mL), SMPs (50 mg) were then suspended in the DOX solution and stirred at dark for 24 h. The DOX-loaded particles (DOX@SMPs) were washed with water for three times, and then were collected by centrifugation and lyophilization. To determine the DOX loading efficiency, the supernatant was collected and the unloaded DOX was measured using a UV–Vis spectrophotometer.

The MON coating was performed as previously described [41]. Briefly, DOX@SMPs (5 mg) were suspended in distill water (0.5 ml), the dispersion was vigorously mixed for 15 s after individual addition of $FeCl_3{\cdot}6\ H_2O$ solution (2.5 μL, 10 mg/mL) and tannic acid (2.5 μL, 40 mg/mL). The molar ratio of ferric iron to tannic acid is 1.58:1. Then, Tris buffer (20 mM, pH 8.0, 0.5 mL) were added immediately into the solution followed by ultrasonic dispersion for 5 min. The microparticles were washed, collected and stored in fridge (−20 °C) for further use. The microparticles with different coating cycles of TA-Fe^{3+} coordination networks were obtained by repeating above steps.

2.5. Characterization

The microscope and fluorescence images of SMPs were observed using a fluorescence microscope (Olympus, Japan), and the size distribution of SMPs were statistically obtained. The surface morphologies of SMPs and SMPs-MON were explored by scanning electron microscopy (JSM-5610LV, Japan) and transmission electron microscopy (Hitachi-HT7700, Japan). The zeta potentials of SMPs and SMPs-MON were measured by Zetasizer Nano-ZS 3600 (Malvern, UK). The secondary structures of SMPs and SMPs-MON were recorded by FTIR spectroscopy (Nicolet iS10 spectrometer, Thermo Fisher). The photoluminescent property of SMPs and SMPs-MON were measured using a RF-6000 PC fluoro spectrophotometer. The Fe contents of SMPs-MON were characterized using ICP-AES (iCAP 7000 Series ICP Spectrometer).

2.6. Hemolysis assay

The hemolysis activities of microparticles were examined according to previous work [43]. Red blood cells (RBCs, 900 μL, 2% in PBS) were mixed with microparticle suspensions (100 μL, in PBS). The mixtures were incubated in 37 °C for 4 h, then centrifuged at 9000 rpm for 10 min. The absorption of supernatant was measured using Thermoscientific NanoDrop 2000 Spectrophotometer at 545 nm. TritonX-100 (1%, v/v) and PBS were served as positive and negative controls, respectively.

2.7. In vitro drug release behaviors

The DOX-loaded microparticles (DOX@SMPs and DOX@SMPs-MON, 1 mg) were dispersed in the buffers (2 mL) with different pH values (acetate buffer, pH 5.0; PBS, pH 6.5 or pH 7.4), respectively. The mixtures were violently shaken at 37 °C. At different time intervals (0, 3, 6, 12, 24, 48, 72 h), the supernatant was collected to measure the released DOX, and fresh buffers were replenished.

The pH-responsiveness of SMPs-MON was also studied in the buffers with different pH values (5.0, 6.5 and 7.4). Briefly, SMPs-MON (2 mg) were dispersed in the buffers (4 mL) and incubated with shaking at 37 °C. At different time intervals (12, 24 and 48 h), the microparticles were collected and characterized by ICP-AES to study the Fe contents.

2.8. Cell culture and animals

Murine mammary carcinoma cells (4T1) were cultured in Roswell Park Memorial Institute (RPMI) 1640 media containing FBS (10%) in an incubator of 5% CO_2 and at 37 °C. Murine macrophage-like cells (RAW 264.7) and human embryonic kidney cells (293T) were cultured in Dulbecco's Modified Eagle's Medium (DMEM) containing FBS (10%) in an incubator of 5% CO_2 and at 37 °C.

Female BALB/c mice (4–6 weeks, 18–20 g) were obtained from SPF (Beijing) biotechnology co., LTD, and raised in specific pathogen free housing conditions. All the animal studies were approved by the animal care and use committee of Huazhong University of Science and Technology (Wuhan, China), and deferred to the protocols approved by the ethics committee of Tongji Medical College, Huazhong University of Science and Technology (Wuhan, China).

2.9. In vitro immunotoxicity assay

RAW264.7 cells were seeded on 8 mm^2 glass coverslips in a 12-well plate at the density of 10000 cells/well in DMEM with 10% FBS, and cultured for 24 h. The media were replaced with fresh media containing sericin, SMPs, SMPs-MON (200 μg/mL) or lipopolysaccharide (1 μg/mL, LPS). After incubating for 24 h, the cells were washed with PBS for three times and fixed with 4% paraformaldehyde. Then, the cells were stained successively with FITC-phalloidim for 25 min and Hoechst 33342 for 15 min. The coverslips were taken out and the cells were observed by a Nikon Ti–U microscope equipped with a CSU-X1 spinning disk confocal unit (Yokogawa) and an EM-CCD camera (iXon+; Andor). The cells treated with PBS were set as the negative control. The green fluorescence intensity was randomly selected from over 200 cells and quantified by Image J software.

The total mRNA of the RAW264.7 cells receiving different treatments was extracted using Trizol reagent and then conversed to cDNA according to the manufacturer's directions. Then, the qRT-PCR was performed on ABI StepOne Plus Detector System using SYBR Green qPCR Master Mix successively (Vazyme Biotech, China). The relative mRNA levels were normalized using GAPDH. The primers are listed in Table S1.

2.10. In vitro cellular uptake

The cellular uptake behavior of DOX@SMP-MON was evaluated using confocal laser scanning microscope (CLSM) and flow cytometry. 4T1 cells were seeded in a 12-well plate at the density of 8000 cells/well and incubated for 24 h. Then, the cells were incubated in the media containing free DOX, DOX@SMPs or DOX@SMPs-MON (3 μg/mL of DOX) for 4 or 6 h. For CLSM imaging, the cells were washed with cold PBS for three times, fixed with 4% paraformaldehyde, stained with Hoechst 33342, and then observed by CLSM. For flow cytometry, the cells were washed with PBS, trypsinized, and collected by centrifugation, and then analyzed by flow cytometry (BD LSRFortessa X-20).

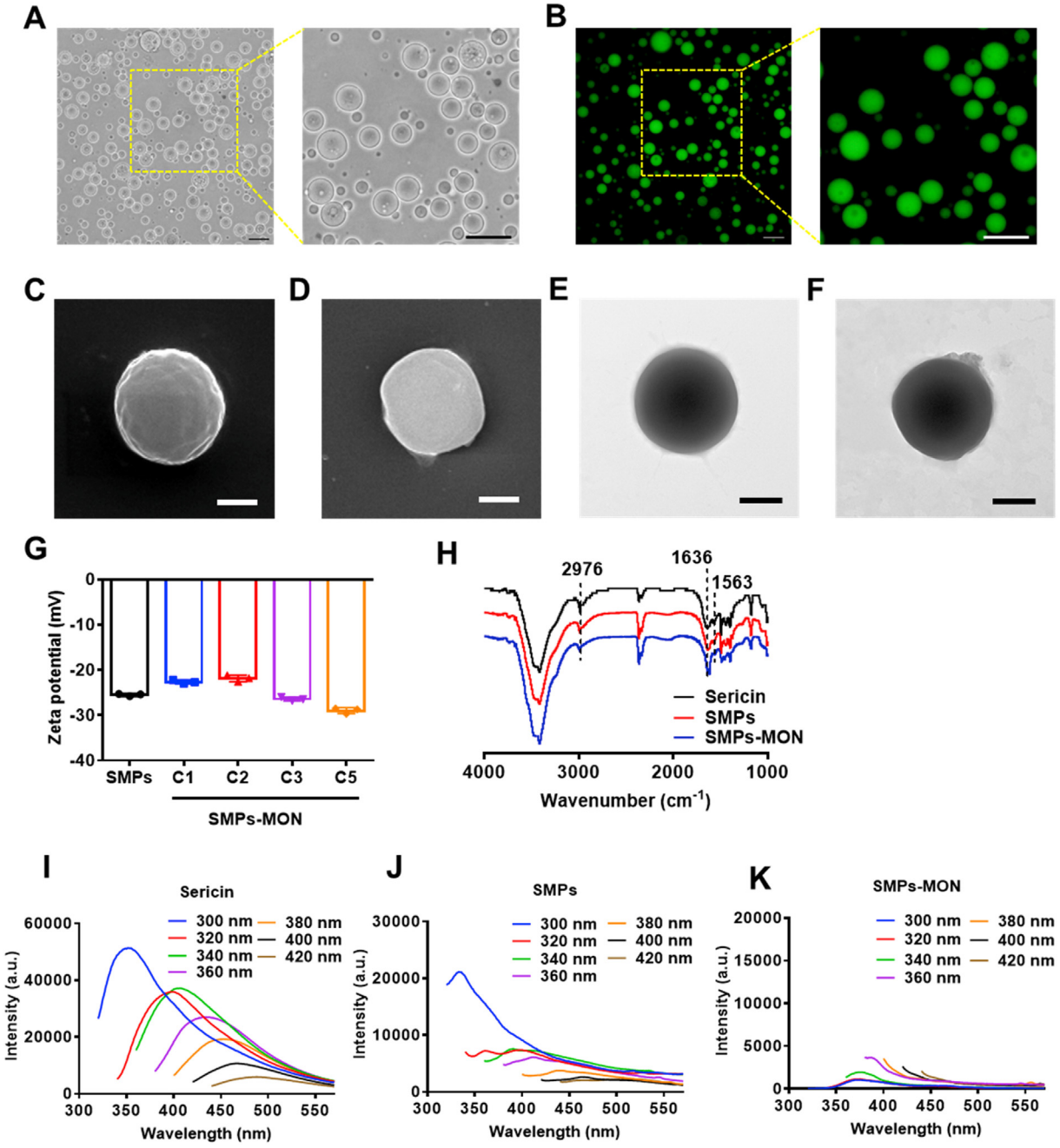

Fig. 1. Characterizations of microparticles. (A, B) The microscopic (A) and fluorescence microscopic (B) images of SMPs. Scale bars, 20 μm. (C, D) SEM images of SMPs (C) and SMPs-MON (D). Scale bars, 1 μm. (E, F) TEM images of SMPs (E) and SMPs-MON (F). Scale bars, 1 μm. (G) Zeta potentials of SMPs before and after TA-Fe^{3+} networks coating. (H) FTIR of Sericin, SMPs and SMPs-MON. (I–K) The emission spectra of Sericin (I), SMPs (J) and SMPs-MON (K).

2.11. Cytotoxicity assay in vitro

4T1 cells were cultured in 96-well plates at the density of 8000 cells/well, and incubated for 24 h. The media were replaced with fresh media containing free DOX, DOX@SMPs or DOX@SMPs-MON. After incubation for 24 or 48 h, the media were replaced with fresh media (200 μL) and 3-(4,5-dimethyl-2-thiazolyl)-2,5-diphenyl-2-H-tetrazolium bromide reagent (MTT) (5 mg/mL in PBS, 20 μL). After 4-h incubation, the solutions were replaced with DMSO to dissolve the formazan crystals. The absorbance was measured at 490 nm (OD value) by a microplate reader (Infinite F50, Tecan, Switzerland). The cell viability was calculated as: cell viability (%) = $(OD_{sample}-OD_{blank})/(OD_{control}-OD_{blank}) \times 100\%$.

2.12. Lung deposition of DOX@SMPs-MON

Female BALB/c mice were anesthetized, free DOX solution or DOX@SMPs-MON suspension (50 μL, 5 mg/kg of DOX) were directly injected into the trachea using an intravenous catheter (22G). To recognized the lung deposition, mice administrated with free DOX or DOX@SMPs-MON were sacrificed at 1, 3, 5 and 10 days post-administration and the lung tissues were visualized using In-Vivo FX PRO (Bruker, GER) at excitation and emission wavelengths of 530 and 600 nm, respectively.

2.13. In vivo antitumor activity on lung metastatic tumors

To establish the 4T1 metastatic tumor model, female BALB/c mice

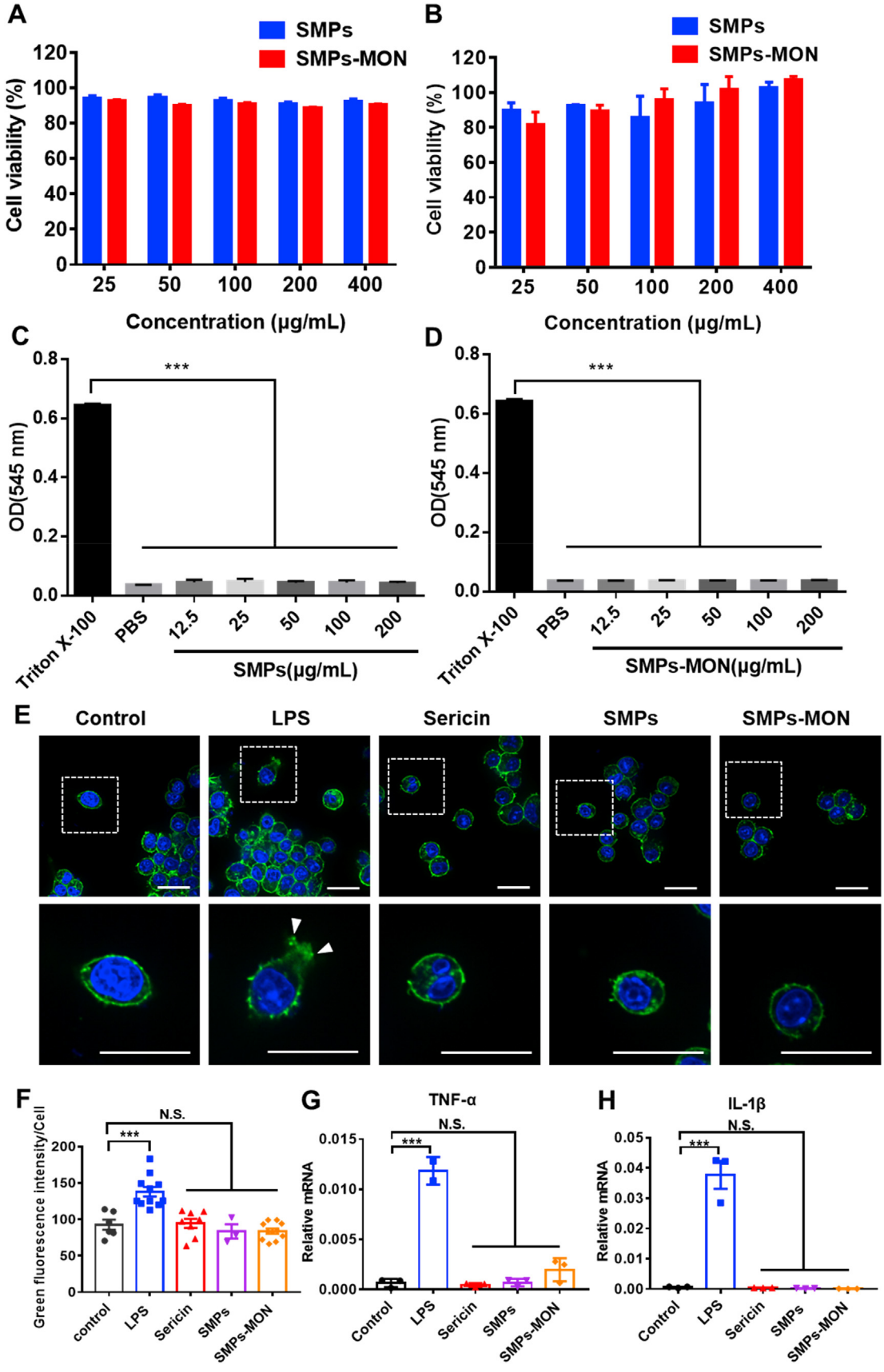

Fig. 2. Biocompatibility of microparticles. (A–B) Cytotoxicity of SMPs and SMPs-MON in 4T1 cells (A) and 293T cells (B) with 48 h incubation. (C–D) The hemolytic activity of SMPs (C) and SMPs-MON (D). (E) The confocal images of RAW264.7 cells treated with LPS, Sericin, SMPs and SMPs-MON for 24 h, respectively. Scale bars, 20 μm. (F) Quantitative analysis of the green fluorescence area (F-actin) per cell receiving different treatments. (G, H) The relative mRNA levels of TNF-α (G) and IL-1β (H) in RAW264.7 cells receiving different treatments.

were intravenously injected with 3×10^5 4T1 cells (100 μL) through tail vein (day 0). To test the anti-tumor efficacy, DOX@SMPs-MON or free DOX (5 mg/kg of DOX) were administered into the trachea of mice on day 7. Mice were sacrificed on day 21, the lung tissues and major organs were isolated. The weight of lung tissues and the number of metastatic pulmonary nodules were measured. In addition, the lung tissues were fixed with 4% paraformaldehyde, embedded with paraffin, sectioned, and stained with hematoxylin-eosin (H&E). The number of metastatic foci and the size of nodules in the H&E images were calculated using Image-Pro Plus (version 6.0, Media Cybernetics, Inc., MD, USA).

2.14. Biochemical analysis

Female BALB/c mice were divided into three groups ($n = 3$), and intratracheal administrated with PBS, free DOX and DOX@SMPs-MON (5 mg/kg of DOX), respectively. After 7 days, mice were sacrificed and the blood samples were collected. The sera were obtained by centrifugation (3500 rpm, 10 min) and analyzed by biochemical assay. Creatine kinase (CK) and lactate dehydrogenase (LDH) were measured to reflect cardiac function. Aspartate aminotransferase (AST) and alanine aminotransferase (ALT) were tested to reflect liver function. Blood urea nitrogen (BUN) and blood uric acid (UA) were measured to reflect renal function. Moreover, the major organs were obtained, fixed and stained.

2.15. Statistical analysis

Statistical analysis was performed using Student's *t*-test. All data were presented as mean ± standard deviation (SD). Statistical significances were conducted as follow: $^*p < 0.05$, $^{**}p < 0.01$, $^{***}p < 0.001$, N.S., not significant.

3. Results

3.1. Preparation and characterization of SMPs-MON

The metal-organic networks enveloped sericin microparticles were simply synthesized via two steps: (1) the sericin microparticles (termed as SMPs) were synthesized by the method of water in oil (w/o) single emulsion using glutaraldehyde as a crosslinker; (2) doxorubicin (DOX), an anticancer drug, was loaded into the SMPs, and then the particles were capped with coordination networks, which were formed by tannic acid (TA, a green tea extractive) and ferric irons (Fe^{3+}). The DOX-loaded microparticles were named as DOX@SMPs-MON (Scheme 1), whereas the microparticles without DOX were referred to as SMPs-MON.

The SMPs possessed a spherical shape with an average diameter of 4.6 ± 1.2 μm (Fig. 1A, Fig. S1). Due to the intrinsic photoluminescent properties of sericin, SMPs exhibited strong green fluorescence (Fig. 1B), confirming the constituents and spherical shapes of microparticles. The scanning electron microscopy (SEM) and transmission electron microscopy (TEM) images also showed the spherical shape of SMPs with a smooth surface (Fig. 1C and E). To control drug release behaviors of microparticles, the TA-Fe^{3+} based metal-organic networks (MON) were coated on the surface of microparticles after drug loading. The color of the microparticles became darker and the Fe contents increased as the cycles of coating increased, indicating that MON is successfully wrapped on the microparticles and the coating thickness is easily controlled by coating cycles (Fig. S2). The SMPs with 2 cycles of MON coating were termed as SMPs-MON, and investigated in further study. As shown in SEM and TEM images, MON coating did not alter the shape of microparticles (Fig. 1D and F), but markedly changed the surface and slightly affected the zeta-potential of particles (−20 mV to −30 mV) (Fig. 1G). The element mapping exhibited the new signal of Fe element in SMPs-MON, confirming the MON coating (Fig. S3). While the coating film formed on SMPs was not homogenous, likely due to the stepwise feeding procedures and fast coordination process, which might be optimized by employing a syringe pump to control the feeding process. FTIR analysis indicates that the crosslinking and MON coating did not change the secondary structure of sericin (Fig. 1H). Then, we examined the photoluminescence properties of sericin-based microparticles. SMPs also exhibited fluorescence as well as sericin, while the fluorescence intensity was decreased by crosslinking (Fig. 1I and J). After coating with MON, the fluorescence of SMPs-MON was significantly weakened, likely because of the quenching effect derived from the TA-Fe^{3+} coordination coating (Fig. 1K).

3.2. In vitro biocompatibility of SMPs-MON

Good biocompatibility is crucial for an ideal drug carrier in biomedical applications [44]. The cytotoxicity of SMPs and SMPs-MON were tested in 4T1 and 293T cells. After incubation for 48 h with these microparticles, the viability of cells was higher than 90% at the concentration of 400 μg/mL (Fig. 2A and B), indicating the good cytocompatibility of sericin-based microparticles. Moreover, SMPs and SMPs-MON exhibited extremely low hemolytic activity even at the concentration of 200 μg/mL (Fig. 2C, D and Fig. S4), suggesting their good hemo-compatibility.

Further, the immunotoxicity of SMPs and SMPs-MON was studied in murine macrophage-like cells (RAW264.7), which are sensitive to inflammatory agents by generating F-actin-rich filopodia and filaments [45,46]. The lipopolysaccharides (LPS) treatment activated RAW264.7 cells, causing significantly polarization with abundant filopodia and membrane spreading. In sharp contrast, SMPs and SMPs-MON treatments did not change the cellular morphology, similar to the cells treated with PBS (Fig. 2E and F). Consistently, SMPs and SMPs-MON did not increase mRNA levels of TNF-α and IL-1β, two key inflammatory cytokines indicating the activation of macrophages (Fig. 2G and H). Taken together, these results indicate that SMPs and SMPs-MON have good biocompatibility *in vitro*.

3.3. In vitro pH-responsive drug release kinetics

Doxorubicin (DOX) as a model anticancer drug was loaded into the microparticles. The drug encapsulation efficiency (EE) and loading content (LC) in DOX@SMPs were 74.35% and 15.86%, respectively. After MON coating, few of DOX molecules (0.45%) were leaked from the microparticles, the loading content slightly decreased to be 15.70% in DOX@SMPs-MON. To investigate the pH-responsive drug release behaviors of DOX and encapsulation effects of MON, the DOX-loaded microparticles were incubated in buffers with different pH values, resembling blood and normal tissues (pH 7.4), tumor microenvironment (pH 6.5), and intracellular lysosomes (pH 5.0). The DOX release rate from DOX@SMPs was dependent on the pH values, as the cumulative release amount of DOX reached 86.3% at pH 5.0 within 72 h, which is significantly higher than that at pH 7.4 (37.2%), likely because that acidic conditions decreased the electrostatic interactions between SMPs and DOX, and increased the hydrophilic property of DOX (Fig. 3A). Notably, MON significantly decreased the release rates of DOX at all the pH conditions (Fig. 3B), and the decreasing degree is highly correlative with the coating cycles of MON on microparticles (Figs. S5A–C), indicating that MON coating effectively facilitates controlling drug release and sustaining DOX release. Moreover, the DOX release rates at acidic conditions were higher than that at neutral condition, likely because of MON disassembly by protonation of hydroxyl groups on TA (Fig. S5D) [41].

3.4. In vitro cellular uptake

To explore cellular uptake efficiency of DOX-loaded microparticles, murine breast cancer cells (4T1) were exposed to DOX@SMPs or DOX@

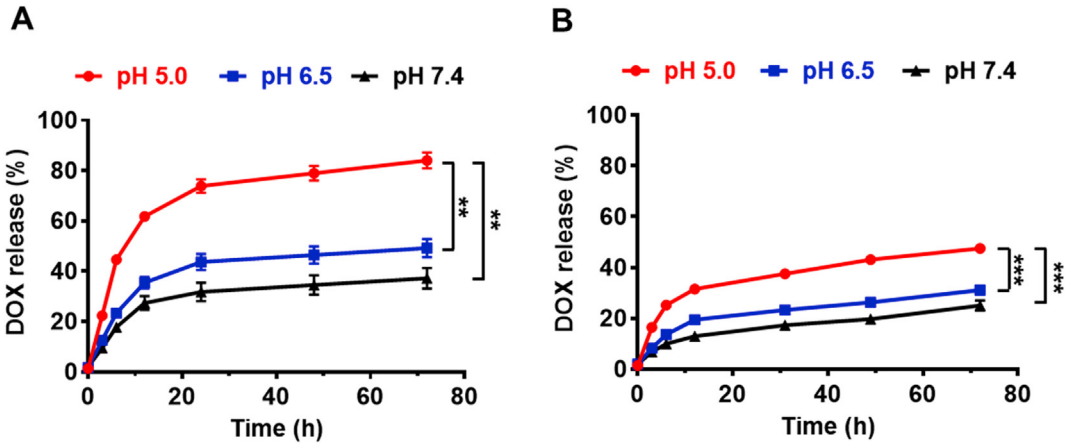

Fig. 3. Cumulative release of DOX from DOX-loaded microparticles *in vitro*. (A–B) The release of DOX from DOX@SMPs (A) and DOX@SMPs-MON (B) in the buffers with different pH values (pH 5.0, pH 6.5 and pH 7.4).

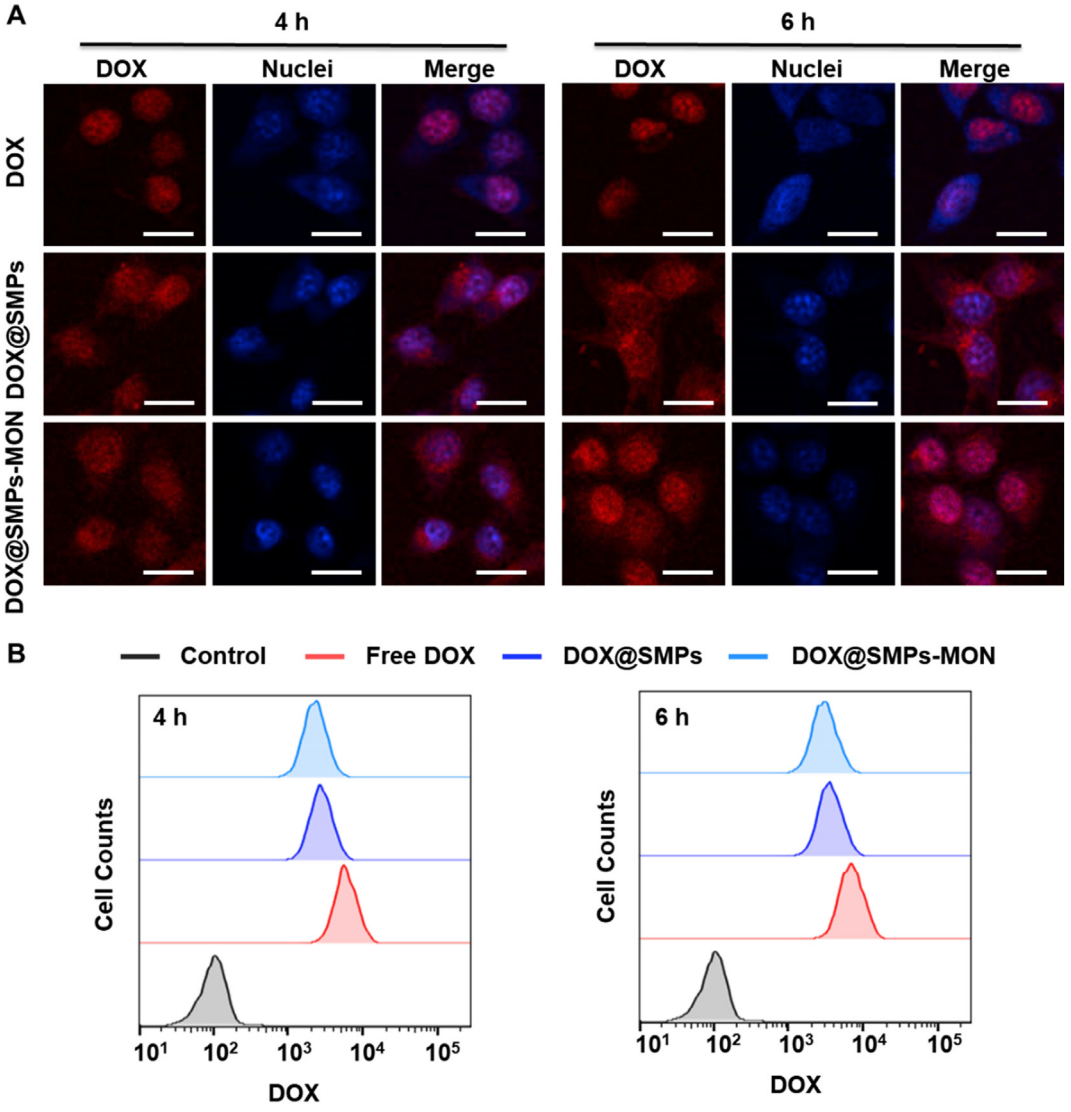

Fig. 4. Intracellular uptake of DOX@SMPs-MON. (A) The confocal images of 4T1 cells treated with free DOX, DOX@SMPs and DOX@SMPs-MON (5 μg/mL of DOX) for 4 h and 6 h. Scale bars, 20 μm. (B) Flow cytometry analysis of 4T1 cells treated with free DOX and DOX@SMPs-MON (5 μg/mL of DOX) for 4 h and 6 h.

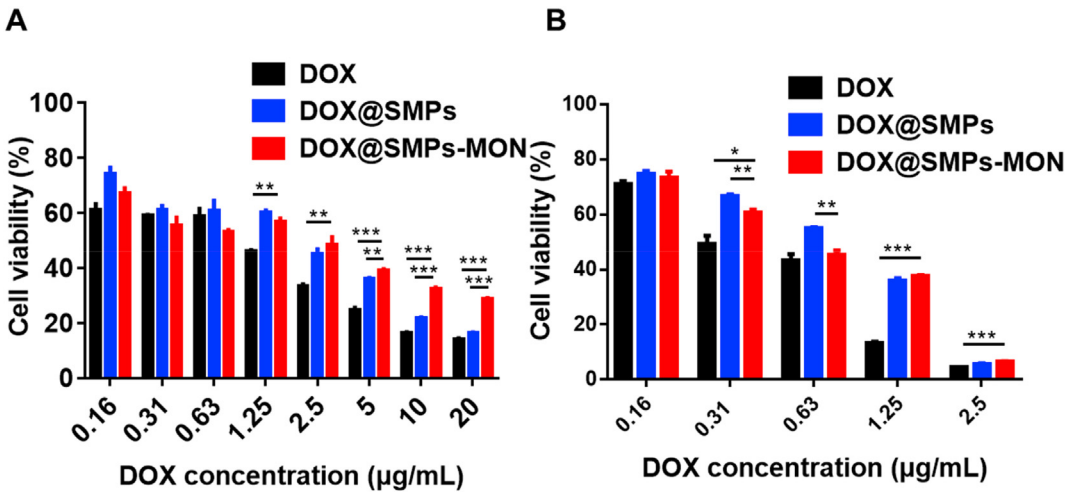

Fig. 5. *In vitro* antitumor effects of DOX@SMPs-MON. Cytotoxicity evaluations of DOX, DOX@SMPs and DOX@SMPs-MON incubating with 4T1 cells for 24 h (A) and 48 h (B).

SMPs-MON for 4 or 6 h, and then were analyzed using confocal and flow cytometry. Obviously, the microparticles delivered DOX into tumor cells, and the internalization amount increased with prolonged incubation time (Fig. 4A and B). Unlike the free DOX that mainly located in the cell nuclei, the DOX fluorescence were observed in both of cytoplasm and nuclei in the cells exposed to DOX@SMPs or DOX@SMPs-MON for 4 h. The MON coating did not significantly affect the cellular uptake efficacy of the DOX-loaded microparticles (Fig. 4A and B). Of note, more DOX fluorescence could be observed in cell nuclei after longer incubation (6 h) (Fig. 4A), suggesting that DOX is released intracellularly and enters nuclei, causing cytotoxicity.

3.5. In vitro antitumor activity of DOX@SMPs-MON

The antitumor effects of DOX@SMPs-MON were studied in 4T1 cells. The viability of cells exposed to DOX-based formulations was reduced in a dose dependent manner (Fig. 5A and B). Free DOX exhibited stronger antitumor effects than DOX-loaded microparticles against 4T1 cells *in vitro*, due to effective cellular internalization and nuclear accumulation of free DOX (Fig. 4A). Under 24 h incubation, the cytotoxicity of DOX@SMPs-MON was weaker than that of DOX@SMPs, it is likely because TA-Fe^{3+} based MON capping decreased DOX release rates.

3.6. Lung deposition of DOX@SMPs-MON

To investigate the distribution of DOX-based formulations *in vivo*, free DOX and DOX@SMPs-MON were administrated directly into trachea of BALB/c mice through an intravenous catheter (Fig. S6), while free DOX administrated by intravenous injection was used as a control. Lung deposition images were observed over 10 days after administration by detecting DOX fluorescence that reflected DOX's distribution and retention in lungs (Fig. 6A and Fig. S7). The DOX accumulation efficacy in lungs was extremely low by intravenous injection of free DOX. Although free DOX could accumulate in lungs through intratracheal administration, the deposited DOX in lungs was cleared quickly within 3 days. In contrast, DOX@SMPs-MON was localized throughout lungs with strong DOX fluorescence and stayed more than 5 days (Fig. 6A and B), indicating that DOX@SMPs-MON effectively accumulates in lungs and chronically releases DOX.

3.7. In vivo antitumor effects and systemic toxicity of DOX@SMPs-MON

To assess the antitumor activity of DOX@SMPs-MON against lung

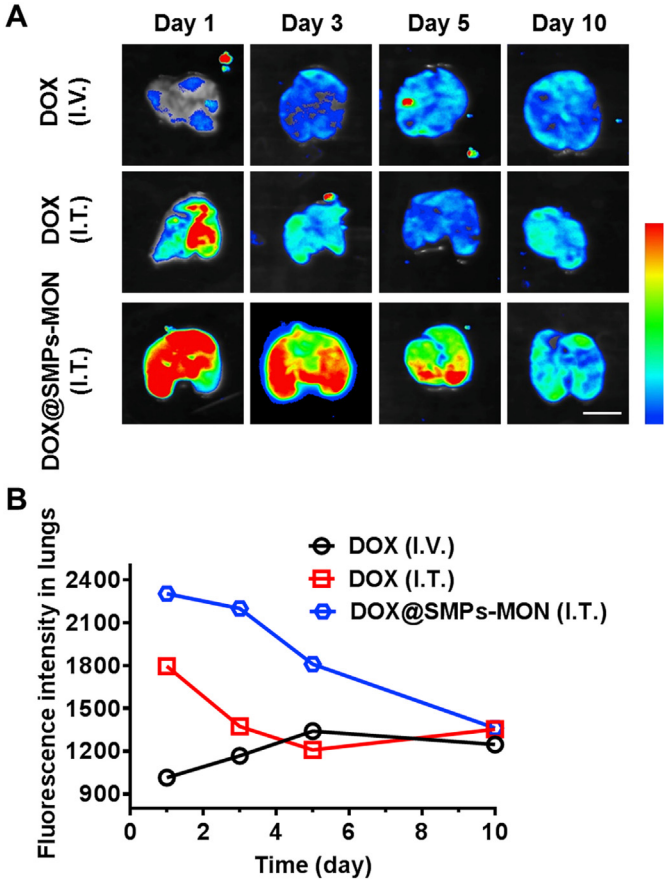

Fig. 6. Lung deposition of DOX@SMPs-MON *in vivo*. (A) Monitoring of the lung deposition of free DOX and DOX@SMPs-MON in BALB/c mice using IVIS imaging system. Scale bars, 1 cm. (B) The fluorescence intensity of DOX in lung tissues after administration.

metastatic cancer, we utilized 4T1 metastatic tumor bearing BALB/c mice as a preclinical animal model [47]. After receiving 4T1 cells (0.3 million) via intravenous injection for 1 week, the mice were treated with PBS, free DOX and DOX@SMPs-MON (5 mg/kg of DOX, 1 time) by intratracheal administration, respectively. At day 21, the mice were sacrificed and lung tissues were isolated (Fig. 7A). Compared with the lungs isolated from the mice receiving PBS treatment, free DOX did not

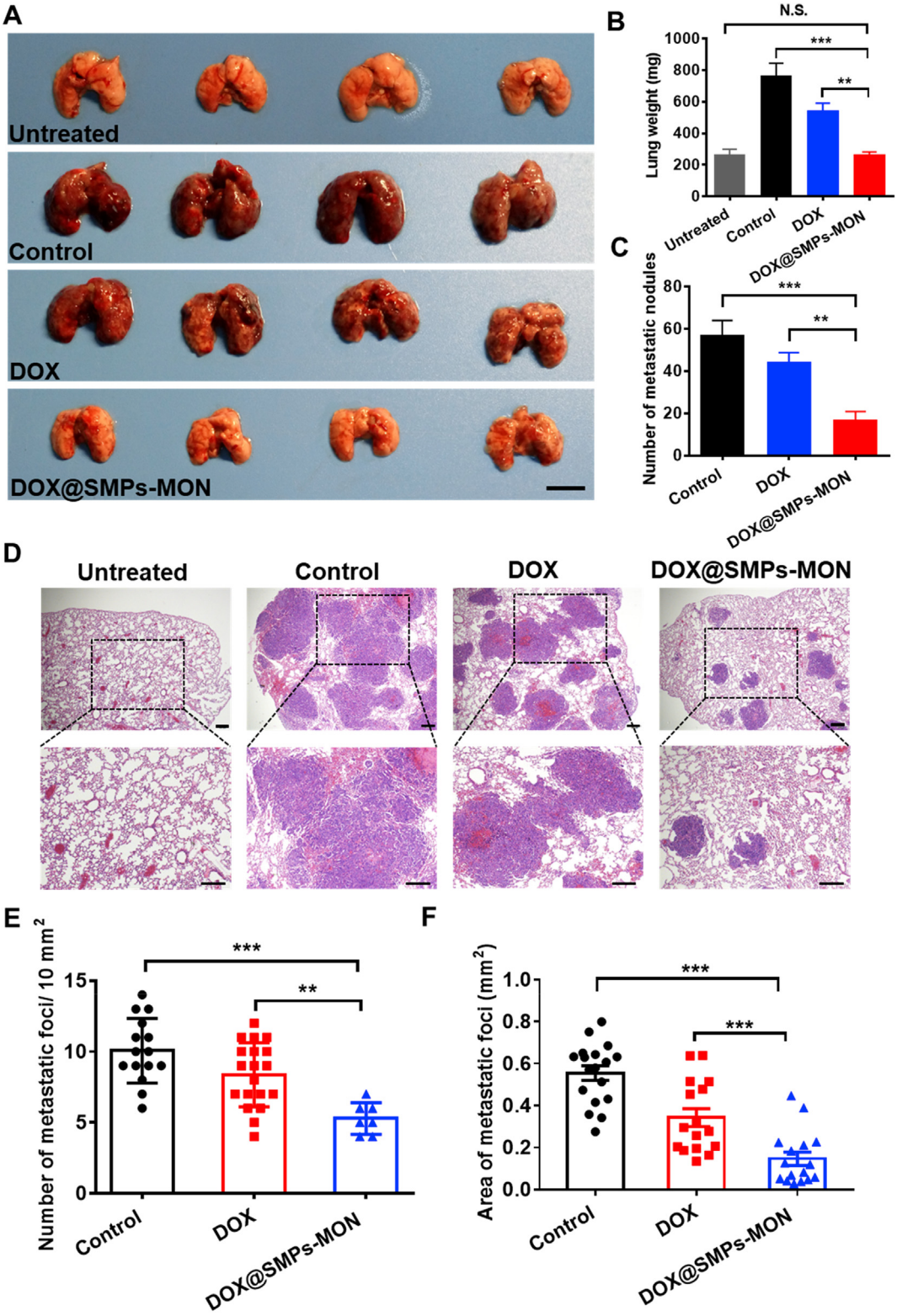

Fig. 7. *In vivo* antitumor effects in lung metastatic 4T1 tumors. (A) The photographs of representative lung tissues isolated from the mice receiving treatments. Scale bars, 1 cm. (B) The average weight of lung tissues isolated from the mice. (C) The number of metastatic lung cancer from the mice. (D) H&E histological staining of lung tissues isolated from the mice receiving treatments. Scale bars, 200 μm. (E–F) Quantification analysis of number (E) and area (F) of metastatic foci in the H&E staining of lung tissues.

significantly decrease lung weight and reduce the number of metastasis foci in lungs. In sharp contrast, DOX@SMPs-MON markedly decreased the lung metastasis nodules by 71% compared to PBS treatment, 3.2-fold more effective than free DOX treatment (Fig. 7B and C). Moreover, the lungs isolated from the mice receiving DOX@SMPs-MON exhibited similar appearances to those in the untreated mice, and the lung weight was also close to the untreated group. Further, the analysis on lung tissues stained with hematoxylin-eosin (H&E) showed that DOX@SMPs-

MON not only reduced the number of metastatic foci, but also decreased the size of nodules (Fig. 7D–F), indicating that DOX@SMPs-MON effectively suppressed lung metastasis.

Remarkably, SMPs-MON suppressed the toxic side effects of DOX, as indicated by (1) DOX@SMPs-MON did not significantly alter the body weight of tumor-bearing mice (Fig. S8); (2) free DOX induced cardiac tissue damages by causing hemolysis and infiltration of inflammatory cells (Fig. S9), while these histopathological alterations were not observed in the major organs of the mice receiving DOX@SMPs-MON; and (3) DOX@SMPs-MON did not impair the functions of major organs (including heart, liver and kidney), but free DOX did (Table S2). All these results suggest that SMPs-MON is an effective and safe pulmonary system for treating metastatic lung cancer in a mouse tumor model.

4. Discussion

Lung, an important organ for breathing, is one of the most frequent targets for cancer metastasis from other tissues or organs [48]. Chemotherapy is the major approach for treating lung cancers, while the systemic administration of chemotherapeutic agents is usually limited by low delivery efficiency and undesirable systemic toxicity [4,49]. Herein, we proposed a pulmonary drug release system based on natural protein for treating metastatic lung cancer. This system is capable of delivering drugs to lung tumors directly, achieving effective retention and sustained drug release in lungs, and suppressing tumor growth with reduced systemic toxicity.

Sericin, a natural protein extracted from silk cocoons, is a versatile biomaterial for drug delivery and tissue engineering due to its excellent bioactivities, including biodegradability, biocompatibility, low-immunogenicity and natural cell adhesion [28,29]. Using a water-in-oil single emulsification method, we have prepared sericin-based microparticles (SMPs) with the average diameter of 4.6 μm. The particles have several advantages as a pulmonary drug delivery system: (1) the SMPs were composed of sericin, thus exhibiting great biocompatibility (Fig. 2); (2) the SMPs effectively encapsulated DOX with an satisfying loading content (15.86%) and high encapsulation efficiency (74.35%); (3) the suitable size of SMPs may help the loaded drugs to be deposited in alveoli and bypass vigorous clearance of alveolar macrophages, leading to effective retention in lungs [50,51]. In addition, we wrapped the microparticles with TA-Fe^{3+} based metal-organic networks (MON) layer by layer to control the drug release rate (Fig. 3). The MON coating was pH sensitive, which keeps them stable in neutral and alkaline conditions, but degrades in acidic environment (Fig. S5D) [52,53]. Thus, the SMPs-MON could prevent premature leakage in normal tissue (under neutral condition), and release cargos in metastasis nodules and cancer cells (under acidic conditions).

The mice in anesthetized state cannot inhale spontaneously microparticles, and the delivery efficiency of nebulization in an inhalation chamber instrument was low and could hardly be controlled [54]. Thus, we directly delivered DOX@SMPs-MON into bronchial airways by intratracheal instillation. One day after administration, DOX@SMPs-MON spread throughout the lungs and stably stayed over 5 days, much longer than free DOX treatment (Fig. 6), likely because of bypassing macrophages and sustained DOX release from the microparticle system.

We further tested the antitumor activity of DOX@SMPs-MON in the metastatic lung tumor based on the 4T1 breast cancer. *In vitro*, SMPs-MON transported DOX into 4T1 cells (Fig. 4), and effectively killed the cancer cells (Fig. 5). In animal experiments, DOX@SMPs-MON markedly reduced the number of metastasis foci and decreased the size of nodules. Remarkably, the appearances and weights of lungs isolated from the mice receiving DOX@SMPs-MON were quite similar with those of the healthy mice (Fig. 7). In contrast, free DOX did not suppress metastasis tumor, but induced systemic toxicity by damaging the functions of major organs in the animal model.

Our work demonstrates that the sericin microparticles with MON coating (SMPs-MON) may serve as a promising pulmonary drug delivery system, featured by good biocompatibility, controlled drug release capability, and great antitumor activity. Given the versatile properties of metal-organic networks, SMPs-MON could be easily post-modified with catechol-terminated targeting ligands and functional groups via self-assembly [41], which may further optimize the sericin-based system by targeting lung metastasis nodules and combination therapies in future.

5. Conclusion

We have designed and fabricated sericin microparticles with TA-Fe^{3+} based coordination film (SMPs-MON) as an effective pulmonary delivery system for treating lung metastatic cancer. The SMPs-MON possesses good biocompatibility, and exhibits high drug encapsulation and sustained drug release property, and thus can serve as a suitable drug carrier for pulmonary delivery. In particular, DOX loaded particles (DOX@SMPs-MON) could deposit and spread in the lungs of BALB/c mice after intratracheal administration and remain locally released over 5 days. In 4T1 metastatic tumor bearing mice, DOX@SMPs-MON significantly reduced lung metastasis nodules and decreased their size, and did not damage the functions of major organs of the recipient animal models. Thus, SMPs-MON might serve as a promising delivery system for treating metastatic lung cancers via pulmonary administration.

CRediT authorship contribution statement

Jia Liu: Data curation, Formal analysis, Investigation, Methodology, Writing - original draft, Writing - review & editing. **Yan Deng:** Data curation, Formal analysis, Investigation, Methodology, Writing - original draft. **Daan Fu:** Investigation. **Ye Yuan:** Investigation. **Qilin Li:** Investigation. **Lin Shi:** Investigation. **Guobin Wang:** Investigation, Methodology, Writing - review & editing, Funding acquisition. **Zheng Wang:** Conceptualization, Formal analysis, Investigation, Methodology, Writing - review & editing, Funding acquisition. **Lin Wang:** Conceptualization, Formal analysis, Investigation, Methodology, Writing - review & editing, Funding acquisition.

Declaration of competing interest

Authors have no conflict of interest.

Acknowledgements

This work was supported by the National Natural Science Foundation of China (81773104, 81773263, 81873931, 81974382 and 21708008), the Natural Science Foundation Program of Hubei Province (2017CFB652 and 2018CFB474), the Fundamental Research Funds for the Central Universities (2017KFYXJJ241), the Integrated Innovative Team for Major Human Diseases Program of Tongji Medical College of HUST, and Health Commission of Hubei Province scientific research project (WJ2019M155), the Graduates' Innovation Fund of Huazhong University of Science and Technology (2019ygscxcy069).

Appendix A. Supplementary data

Supplementary data to this article can be found online at https://doi.org/10.1016/j.bioactmat.2020.08.006.

References

[1] F. Bray, J. Ferlay, I. Soerjomataram, R.L. Siegel, L.A. Torre, A. Jemal, Global cancer statistics 2018: GLOBOCAN estimates of incidence and mortality worldwide for 36 cancers in 185 countries, CA A Cancer J. Clin. 68 (2018) 394–424, https://doi.org/10.3322/caac.21492.

[2] S.L. Wood, M. Pernemalm, P.A. Crosbie, A.D. Whetton, The role of the tumor-microenvironment in lung cancer-metastasis and its relationship to potential therapeutic targets, Canc. Treat Rev. 40 (2014) 558–566, https://doi.org/10.1016/j.

ctrv.2013.10.001.
[3] M. Yousefi, R. Nosrati, A. Salmaninejad, S. Dehghani, A. Shahryari, A. Saberi, Organ-specific metastasis of breast cancer: molecular and cellular mechanisms underlying lung metastasis, Cell. Oncol. 41 (2018) 123–140, https://doi.org/10.1007/s13402-018-0376-6.
[4] S.N. Waqar, D. Morgensztern, Treatment advances in small cell lung cancer (SCLC), Pharmacol. Ther. 180 (2017) 16–23, https://doi.org/10.1016/j.pharmthera.2017.06.002.
[5] S.R.D. Johnston, The role of chemotherapy and targeted agents in patients with metastatic breast cancer, Eur. J. Canc. 47 (2011) S38–S47, https://doi.org/10.1016/S0959-8049(11)70145-9.
[6] H.A. Burris 3rd, Shortcomings of current therapies for non-small-cell lung cancer: unmet medical needs, Oncogene 28 (2009) S4–S13, https://doi.org/10.1038/onc.2009.196.
[7] W.-H. Lee, C.-Y. Loo, D. Traini, P.M. Young, Nano- and micro-based inhaled drug delivery systems for targeting alveolar macrophages, Expet Opin. Drug Deliv. 12 (2015) 1009–1026, https://doi.org/10.1517/17425247.2015.1039509.
[8] O.B. Garbuzenko, A. Kuzmov, O. Taratula, S.R. Pine, T. Minko, Strategy to enhance lung cancer treatment by five essential elements: inhalation delivery, nanotechnology, tumor-receptor targeting, chemo- and gene therapy, Theranostics 9 (2019) 8362–8376, https://doi.org/10.7150/thno.39816.
[9] L. Wu, X. Wen, X. Wang, C. Wang, X. Sun, K. Wang, H. Zhang, T. Williams, A.J. Stacy, J. Chen, A.H. Schmieder, G.M. Lanza, B. Shen, Local intratracheal delivery of perfluorocarbon nanoparticles to lung cancer demonstrated with magnetic resonance multimodal imaging, Theranostics 8 (2018) 563–574, https://doi.org/10.7150/thno.21466.
[10] I. Kim, H.J. Byeon, T.H. Kim, E.S. Lee, K.T. Oh, B.S. Shin, K.C. Lee, Y.S. Youn, Doxorubicin-loaded highly porous large PLGA microparticles as a sustained- release inhalation system for the treatment of metastatic lung cancer, Biomaterials 33 (2012) 5574–5583, https://doi.org/10.1016/j.biomaterials.2012.04.018.
[11] I. Kim, H.J. Byeon, T.H. Kim, E.S. Lee, K.T. Oh, B.S. Shin, K.C. Lee, Y.S. Youn, Doxorubicin-loaded porous PLGA microparticles with surface attached TRAIL for the inhalation treatment of metastatic lung cancer, Biomaterials 34 (2013) 6444–6453, https://doi.org/10.1016/j.biomaterials.2013.05.018.
[12] C. Loira-Pastoriza, J. Todoroff, R. Vanbever, Delivery strategies for sustained drug release in the lungs, Adv. Drug Deliv. Rev. 75 (2014) 81–91, https://doi.org/10.1016/j.addr.2014.05.017.
[13] W. Gao, T. Li, Q.T. Zhou, Pulmonary delivery of nanoparticle chemotherapy for the treatment of lung cancers: challenges and opportunities, Acta Pharmacol. Sin. 38 (2017) 782–797, https://doi.org/10.1038/aps.2017.34.
[14] I. d'Angelo, C. Conte, M.I. La Rotonda, A. Miro, F. Quaglia, F. Ungaro, Improving the efficacy of inhaled drugs in cystic fibrosis: challenges and emerging drug delivery strategies, Adv. Drug Deliv. Rev. 75 (2014) 92–111, https://doi.org/10.1016/j.addr.2014.05.008.
[15] C.L. Tseng, S.Y. Wu, W.H. Wang, C.L. Peng, F.H. Lin, C.C. Lin, T.H. Young, M.J. Shieh, Targeting efficiency and biodistribution of biotinylated-EGF-conjugated gelatin nanoparticles administered via aerosol delivery in nude mice with lung cancer, Biomaterials 29 (2008) 3014–3022, https://doi.org/10.1016/j.biomaterials.2008.03.033.
[16] P. Zarogoulidis, E. Chatzaki, K. Porpodis, K. Domvri, W. Hohenforst-Schmidt, E.P. Goldberg, N. Karamanos, K. Zarogoulidis, Inhaled chemotherapy in lung cancer: future concept of nanomedicine, Int. J. Nanomed. 7 (2012) 1551–1572, https://doi.org/10.2147/IJN.S29997.
[17] I.J. Joye, D.J. McClements, Biopolymer-based nanoparticles and microparticles: fabrication, characterization, and application, Curr. Opin. Colloid Interface Sci. 19 (2014) 417–427, https://doi.org/10.1016/j.ijbiomac.2013.12.017.
[18] W.H. Lee, C.Y. Loo, M. Ghadiri, C.R. Leong, P.M. Young, D. Traini, The potential to treat lung cancer via inhalation of repurposed drugs, Adv. Drug Deliv. Rev. 133 (2018) 107–130, https://doi.org/10.1016/j.addr.2018.08.012.
[19] T. Feng, H. Tian, C. Xu, L. Lin, Z. Xie, M.H. Lam, H. Liang, X. Chen, Synergistic co-delivery of doxorubicin and paclitaxel by porous PLGA microspheres for pulmonary inhalation treatment, Eur. J. Pharm. Biopharm. 88 (2014) 1086–1093, https://doi.org/10.1016/j.ejpb.2014.09.012.
[20] M. Beck-Broichsitter, C. Schweiger, T. Schmehl, T. Gessler, W. Seeger, T. Kissel, Characterization of novel spray-dried polymeric particles for controlled pulmonary drug delivery, J. Contr. Release 158 (2012) 329–335, https://doi.org/10.1016/j.jconrel.2011.10.030.
[21] X. Shi, C. Li, S. Gao, L. Zhang, H. Han, J. Zhang, W. Shi, Q. Li, Combination of doxorubicin-based chemotherapy and polyethylenimine/p53 gene therapy for the treatment of lung cancer using porous PLGA microparticles, Colloids Surf., B 122 (2014) 498–504, https://doi.org/10.1016/j.colsurfb.2014.07.020.
[22] Y. Kang, J. Wu, G. Yin, Z. Huang, X. Liao, Y. Yao, P. Ouyang, H. Wang, Q. Yang, Characterization and biological evaluation of paclitaxel-loaded poly(L-lactic acid) microparticles prepared by supercritical CO2, Langmuir 24 (2008) 7432–7441, https://doi.org/10.1021/la703900k.
[23] S. Alipour, H. Montaseri, M. Tafaghodi, Preparation and characterization of biodegradable paclitaxel loaded alginate microparticles for pulmonary delivery, Colloids Surf., B 81 (2010) 521–529, https://doi.org/10.1016/j.colsurfb.2010.07.050.
[24] K. Fukushige, T. Tagami, M. Naito, E. Goto, S. Hirai, N. Hatayama, H. Yokota, T. Yasui, Y. Baba, T. Ozeki, Developing spray-freeze-dried particles containing a hyaluronic acid-coated liposome-protamine-DNA complex for pulmonary inhalation, Int. J. Pharm. 583 (2020) 119338–119345, https://doi.org/10.1016/j.ijpharm.2020.119338.
[25] Y. Ramot, M. Haim-Zada, A.J. Domb, A. Nyska, Biocompatibility and safety of PLA and its copolymers, Adv. Drug Deliv. Rev. 107 (2016) 153–162, https://doi.org/10.1016/j.addr.2016.03.012.
[26] H. Zhu, F. Yang, B. Tang, X.M. Li, Y.N. Chu, Y.L. Liu, S.G. Wang, D.C. Wu, Y. Zhang, Mesenchymal stem cells attenuated PLGA-induced inflammatory responses by inhibiting host DC maturation and function, Biomaterials 53 (2015) 688–698, https://doi.org/10.1016/j.biomaterials.2015.03.005.
[27] H.M. Abdelaziz, M. Gaber, M.M. Abd-Elwakil, M.T. Mabrouk, M.M. Elgohary, N.M. Kamel, D.M. Kabary, M.S. Freag, M.W. Samaha, S.M. Mortada, K.A. Elkhodairy, J.Y. Fang, A.O. Elzoghby, Inhalable particulate drug delivery systems for lung cancer therapy: nanoparticles, microparticles, nanocomposites and nanoaggregates, J. Contr. Release 269 (2018) 374–392, https://doi.org/10.1016/j.jconrel.2017.11.036.
[28] L. Lamboni, M. Gauthier, G. Yang, Q. Wang, Silk sericin: a versatile material for tissue engineering and drug delivery, Biotechnol. Adv. 33 (2015) 1855–1867, https://doi.org/10.1016/j.biotechadv.2015.10.014.
[29] Z. Wang, Y. Zhang, J. Zhang, L. Huang, J. Liu, Y. Li, G. Zhang, S.C. Kundu, L. Wang, Exploring natural silk protein sericin for regenerative medicine: an injectable, photoluminescent, cell-adhesive 3D hydrogel, Sci. Rep. 4 (2014) 7064–7074, https://doi.org/10.1038/srep07064.
[30] B.B. Mandal, A.S. Priya, S.C. Kundu, Novel silk sericin/gelatin 3-D scaffolds and 2-D films: fabrication and characterization for potential tissue engineering applications, Acta Biomater. 5 (2009) 3007–3020, https://doi.org/10.1016/j.actbio.2009.03.026.
[31] H. Xie, W. Yang, J. Chen, J. Zhang, X. Lu, X. Zhao, K. Huang, H. Li, P. Chang, Z. Wang, L. Wang, A silk sericin/silicone nerve guidance conduit promotes regeneration of a transected sciatic nerve, Adv. Healthc. Mater. 4 (2015) 2195–2205, https://doi.org/10.1002/adhm.201500355.
[32] C. Qi, J. Liu, Y. Jin, L. Xu, G. Wang, Z. Wang, L. Wang, Photo-crosslinkable, injectable sericin hydrogel as 3D biomimetic extracellular matrix for minimally invasive repairing cartilage, Biomaterials 163 (2018) 89–104, https://doi.org/10.1016/j.biomaterials.2018.02.016.
[33] L. Huang, K. Tao, J. Liu, C. Qi, L. Xu, P. Chang, J. Gao, X. Shuai, G. Wang, Z. Wang, L. Wang, Design and fabrication of multifunctional sericin nanoparticles for tumor targeting and pH-responsive subcellular delivery of cancer chemotherapy drugs, ACS Appl. Mater. Interfaces 8 (2016) 6577–6585, https://doi.org/10.1021/acsami.5b11617.
[34] J. Liu, C. Qi, K. Tao, J. Zhang, J. Zhang, L. Xu, X. Jiang, Y. Zhang, L. Huang, Q. Li, H. Xie, J. Gao, X. Shuai, G. Wang, Z. Wang, L. Wang, Sericin/dextran injectable hydrogel as an optically trackable drug delivery system for malignant melanoma treatment, ACS Appl. Mater. Interfaces 8 (2016) 6411–6422, https://doi.org/10.1021/acsami.6b00959.
[35] C. Qi, Y. Deng, L. Xu, C. Yang, Y. Zhu, G. Wang, Z. Wang, L. Wang, A sericin/graphene oxide composite scaffold as a biomimetic extracellular matrix for structural and functional repair of calvarial bone, Theranostics 10 (2020) 741–756, https://doi.org/10.7150/thno.39502.
[36] J. Chen, Y. Zhan, Y. Wang, D. Han, B. Tao, Z. Luo, S. Ma, Q. Wang, X. Li, L. Fan, C. Li, H. Den, F. Cao, Chitosan/silk fibroin modified nanofibrous patches with mesenchymal stem cells prevent heart remodeling post-myocardial infarction in rats, Acta Biomater. 80 (2018) 154–168, https://doi.org/10.1016/j.actbio.2018.09.013.
[37] G. Cheng, Z. Davoudi, X. Xing, X. Yu, X. Cheng, Z. Li, H. Deng, Q. Wang, Advanced silk fibroin biomaterials for cartilage regeneration, ACS Biomater. Sci. Eng. 4 (2018), https://doi.org/10.1021/acsbiomaterials.8b00150 2704-271.
[38] T.T. Cao, Y.Q. Zhang, Processing and characterization of silk sericin from Bombyx mori and its application in biomaterials and biomedicines, Mater. Sci. Eng. C 61 (2016) 940–952, https://doi.org/10.1016/j.msec.2015.12.082.
[39] H. Ejima, J.J. Richardson, F. Caruso, Metal-phenolic networks as a versatile platform to engineer nanomaterials and biointerfaces, Nano Today 12 (2017) 136–148, https://doi.org/10.1016/j.nantod.2016.12.012.
[40] K.A. Duck, J.R. Connor, Iron uptake and transport across physiological barriers, Biometals 29 (2016) 573–591, https://doi.org/10.1007/s10534-016-9952-2.
[41] H. Ejima, J.J. Richardson, K. Liang, J.P. Best, M.P. van Koeverden, G.K. Such, J. Cui, F. Caruso, One-step assembly of coordination complexes for versatile film and particle engineering, Science 341 (2013) 154–157, https://doi.org/10.1126/science.1237265.
[42] P. Aramwit, T. Siritientong, T. Srichana, Potential applications of silk sericin, a natural protein from textile industry by-products, Waste Manag. Res. 30 (2012) 217–224, https://doi.org/10.1177/0734242X11404733.
[43] J. Liu, X. Liu, Y. Yuan, Q. Li, B. Chang, L. Xu, B. Cai, C. Qi, C. Li, X. Jiang, G. Wang, Z. Wang, L. Wang, Supramolecular modular approach toward conveniently constructing and multifunctioning a pH/redox dual-responsive drug delivery nanoplatform for improved cancer chemotherapy, ACS Appl. Mater. Interfaces 10 (2018) 26473–26484, https://doi.org/10.1021/acsami.8b05232.
[44] P. Aggarwal, J.B. Hall, C.B. McLeland, M.A. Dobrovolskaia, S.E. McNeil, Nanoparticle interaction with plasma proteins as it relates to particle biodistribution, biocompatibility and therapeutic efficacy, Adv. Drug Deliv. Rev. 61 (2009) 428–437, https://doi.org/10.1016/j.addr.2009.03.009.
[45] G. Luo, B.C. Cheng, H. Zhao, X.Q. Fu, R. Xie, S.F. Zhang, S.Y. Pan, Y. Zhang, Schisandra chinensis lignans suppresses the production of inflammatory mediators regulated by NF-kappaB, AP-1, and IRF3 in lipopolysaccharide-stimulated RAW264.7 cells, Molecules 23 (2018) 3319–3335, https://doi.org/10.3390/molecules23123319.
[46] W.F. Chiou, A.Y.C. Shum, C.H. Peng, C.F. Chen, C.J. Chou, Piperlactam S suppresses macrophage migration by impeding F-actin polymerization and filopodia extension, Eur. J. Pharmacol. 458 (2003) 217–225, https://doi.org/10.1016/s0014-2999(02)02733-4.
[47] B.A. Pulaski, S. Ostrand-Rosenberg, Mouse 4T1 breast tumor model, Curr. Protoc.

Immunol. 39 (2000) 20.2.1–20.2.16, https://doi.org/10.1002/0471142735.im2002s39.
[48] H.H. Popper, Progression and metastasis of lung cancer, Canc. Metastasis Rev. 35 (2016) 75–91, https://doi.org/10.1007/s10555-016-9618-0.
[49] Q. Wang, H. Cheng, H. Peng, H. Zhou, P.Y. Li, R. Langer, Non-genetic engineering of cells for drug delivery and cell-based therapy, Adv. Drug Deliv. Rev. 91 (2015) 125–140, https://doi.org/10.1016/j.addr.2014.12.003.
[50] R. Vanbever, J.D. Mintzes, J. Wang, Formulation and physical characterization of large porous particles for inhalation, Pharm. Res. (N. Y.) 16 (1999) 1735–1742, https://doi.org/10.1023/a:1018910200420.
[51] M.J. Kwon, J.H. Bae, J.J. Kim, K. Na, E.S. Lee, Long acting porous microparticle for pulmonary protein delivery, Int. J. Pharm. 333 (2007) 5–9, https://doi.org/10.1016/j.ijpharm.2007.01.016.
[52] J. Guo, Y. Ping, H. Ejima, K. Alt, M. Meissner, J.J. Richardson, Y. Yan, K. Peter, D. von Elverfeldt, C.E. Hagemeyer, F. Caruso, Engineering multifunctional capsules through the assembly of metal-phenolic networks, Angew. Chem., Int. Ed. Engl. 53 (2014) 5546–5551, https://doi.org/10.1002/anie.201311136.
[53] Y. Luo, B. Qiao, P. Zhang, C. Yang, J. Cao, X. Yuan, H. Ran, Z. Wang, L. Hao, Y. Cao, J. Ren, Z. Zhou, TME-activatable theranostic nanoplatform with ATP burning capability for tumor sensitization and synergistic therapy, Theranostics 10 (2020) 6987–7001, https://doi.org/10.7150/thno.44569.
[54] J. Conde, F. Tian, Y. Hernandez, C. Bao, D. Cui, K.P. Janssen, M.R. Ibarra, P.V. Baptista, T. Stoeger, J.M. de la Fuente, In vivo tumor targeting via nanoparticle-mediated therapeutic siRNA coupled to inflammatory response in lung cancer mouse models, Biomaterials 34 (2013) 7744–7753, https://doi.org/10.1016/j.biomaterials.2013.06.041.